Effect of fracture energy estimation on the predictions of mode II behavior of bonded joints using cohesive zone models

Michele Perrella, Enrico Armentani
Department of Chemical, Materials and Production Engineering, University of Napoli Federico II, Napoli, 80125, Italy
michele.perrella@unina.it, https://orcid.org/0000-0002-3617-2328
enrico.armentani@unina.it, https://orcid.org/0000-0002-3511-6121

Giuseppe Lamanna
Department of Engineering, University of Campania "Luigi Vanvitelli", Aversa (CE), 810131, Italy
giuseppe.lamanna@unicampania.it, http://orcid.org/0000-0002-6282-2224

Valentino Paolo Berardi
Department of Industrial Engineering, University of Salerno, Via Giovanni Paolo II 132, Fisciano (SA), Italy
berardi@unisa.it, https://orcid.org/0000-0002-0008-4828

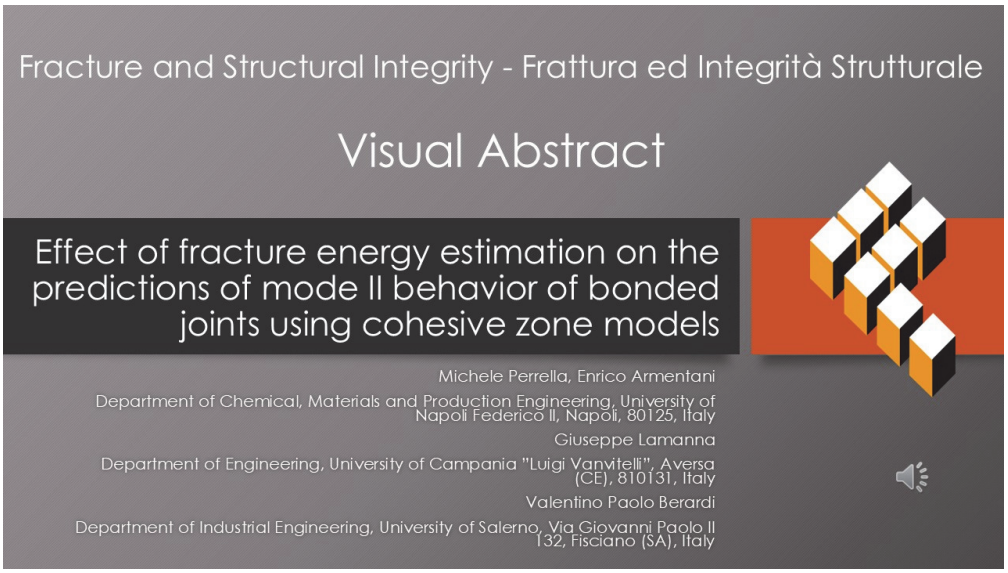

Citation: Perrella, M., Armentani, E., Lamanna, G., Berardi, V. P., Effect of fracture energy estimation on the predictions of mode II behavior of bonded joints using cohesive zone models, Fracture and Structural Integrity, 72 (2025) 236-246.

Received: 24.02.2025
Accepted: 19.03.2025
Published: 23.03.2025
Issue: 04.2025

KEYWORDS. Bonded joint, Finite Element Method (FEM), Cohesive Zone Model (CZM), Digital Image Correlation (DIC), End Notched Flexure (ENF) test.

INTRODUCTION

Currently, structural elements of complex geometry for industrial, automotive, marine, aerospace and civil purposes are realized by means of adhesively bonded joints [1-4]. Among the joining techniques, adhesive bonding offers some advantages over traditional methods, providing the possibility to glue identical and dissimilar materials,

allowing uniform stress distribution along the adhesive layer, reducing the weight of the assembly and consequently its energy consumption [5].

The cohesive zone model (CZM) is popular in literature for providing reliable predictions of interface behavior of adhesively bonded joints for structural and industrial applications, defining a process zone without stress singularity at the crack front [6]. The CZM approach describes the behavior of bonded joints by means of a relationship between traction and separation of adhesive interface. With this aim, many CZM laws have been proposed in literature. Some of them, such as the triangular and the trapezoidal traction-separation (TS) laws, compute damage phenomenon after the occurrence of a maximum cohesive stress value and start a softening stage up to full debonding. Whereas, others, such as the exponential [7], the polynomial [8] and the interpolation-based TS equations [9], manage the calculation of damage parameter directly from the beginning of decohesion process. Different CZM shapes are adopted to better describe the diverse behavior of dissimilar adhesives [10], both ductile and brittle. Although very useful in numerical analysis from a computation standpoint, imposing a priori a TS law shape can influence the prediction of bonded joint decohesion response. Many papers deal with simulations on single lap joint test and double cantilever beam test to highlight the sensitivity of results to CZM shape [11-13]. Other authors analyzed how the TS relationship affected the response of ENF tests [14] and specimens with various geometries made from different materials [15,16]. Therefore, an appropriate identification of TS law is crucial to obtain a proper prediction of strength of bonded joints. Within this context, the direct measurement of CZM parameters is a suitable approach [17]. A very used methodology is based on the derivative of Rice's J-integral as described by Li and Ward [18] and developed by many researchers [19, 20]. Iterative methods for CZM identification without imposing a pre-defined cohesive law shape have been also presented in literature [21, 22]. The application of the direct method requires the decohesion advance acquisition by using vision systems, usually in combination with digital image correlation (DIC) technique. A different approach, named compliance-based beam method (CBBM), was developed in order to avoid uncertainness in such an estimation. The CBBM, based on equivalent crack length concept, is directly related to global load and displacement test machine outputs, hence the monitoring of crack propagation is not necessary.

In this paper, direct methodologies, based on different modelling of SERR, for the identification of CZM law of ENF test are presented. The mode II cohesive TS relationship was obtained through numerical differentiation of SERR and an analytical description of cohesive interface behavior was found via minimization procedure. Numerical predictions, carried out by using CZM laws identified with direct methods, were compared with experimental response in [23], pointing out the differences of such approaches in the assessment of decohesion of bonded joints under mode II loading condition.

MATERIALS

The End Notch Flexure (ENF) test presented in [23] was used to numerically analyse the behaviour of bonded joint under mode II fracture loading condition.

The geometry of adopted ENF specimen is shown in Fig. 1, where B is its width, h is the adherend thickness, L_t is the overall specimen length, L is the span, a_0 is the distance from the support to the pre-crack tip, x_a and x_m are the axial locations of insert edge and of loading point, respectively.

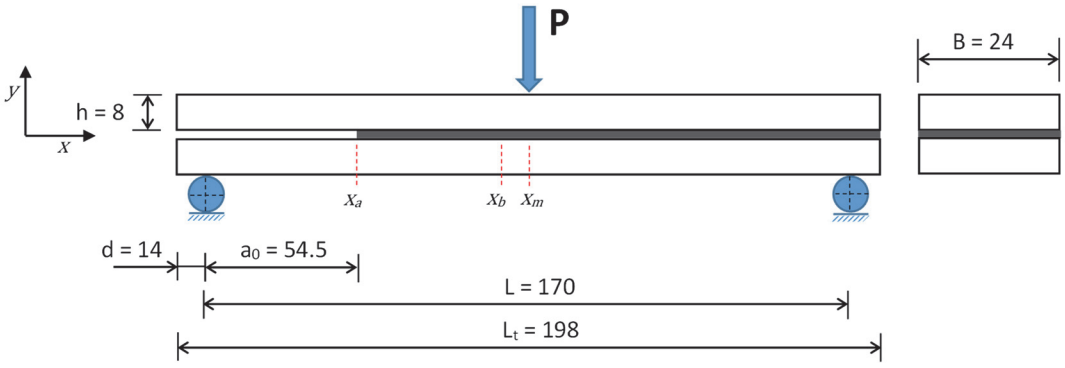

Figure 1: ENF specimen for mode II test (all the dimensions are in mm).

The mechanical properties of Loctite Hysol 3421 A&B by Henkel resin and Al6061 T6 adherend materials are listed in Tab. 1, where E is the Young's modulus, ν is the Poisson's ratio, σ_r is the ultimate tensile stress and σ_y is the yield stress.

Material	E [GPa]	ν [-]	σ_y [MPa]	σ_r [MPa]
Al6061 T6	68	0.33	265	309
Hysol 3421 A&B	0.998	0.34	-	18.6

Table 1: Mechanical properties of the adopted materials.

DIRECT IDENTIFICATION METHODS OF CZM PARAMETERS

The behavior of decohesion of bonded joints can be described with cohesive zone model by traction-separation laws. Direct methodologies for the identification of CZM parameters can better, although non easier, carry out the effective and specific shape of relationship between cohesive stress and displacement jump of adhesive interface.
In the following, some direct approaches are discussed and compared, as well as with the experimental data in [23], also obtained by acquiring displacement fields via DIC technique (see Fig. 2).

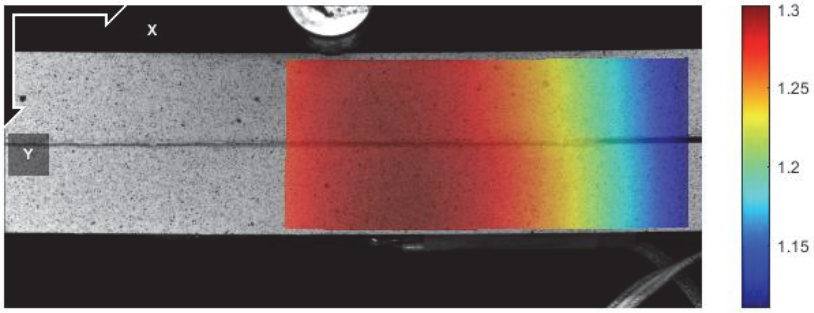

Figure 2: Vertical displacement field obtained by DIC analysis.

Experiments showed a quasi-brittle behavior of bonded joints. Fracture surfaces observed on post mortem samples generally showed an adhesive failure type, as reported in Fig. 3.

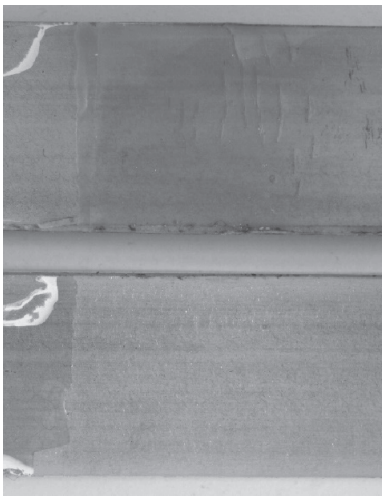

Figure 3: Fracture surfaces from precrack edge to pin loading zone of a representative ENF specimen.

Direct method DIR1: evaluation of simplified fracture toughness by means of J-integral

The identification of CZM parameters can be achieved by avoiding imposing an a priori traction-separation law and using only the experimental data provided by testing machine and DIC analysis. The methodology DIR1 is based on experimental *J*-integral, *J*, evaluation.
The flowchart of DIR1 approach is shown in Fig. 4.

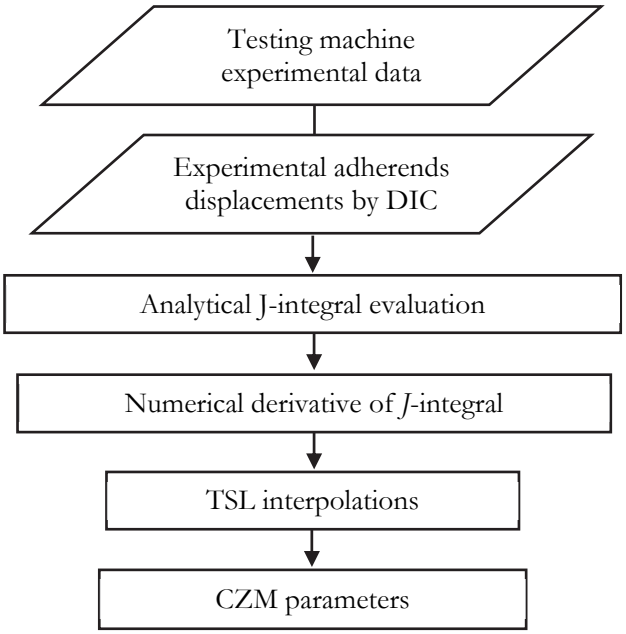

Figure 4: Flowchart of DIR1 approach.

The value of strain energy release rate, G, considering materials as linear elastic, can be obtained from the calculation of J, by using the simplified equation by Leffler et al. [24]:

$$G = J(\delta_s) \cong \frac{9}{16} \cdot \frac{(P \cdot a_0)^2}{EB^2h^3} + \frac{3}{8} \cdot \frac{P \cdot \delta_s}{Bh} \tag{1}$$

where P is the applied load, a_0 is the pre-crack length, δ_s is the tangential displacement of adhesive layer at pre-crack tip, E is the adherend Young's modulus, B and h are respectively the width and thickness of adherends.

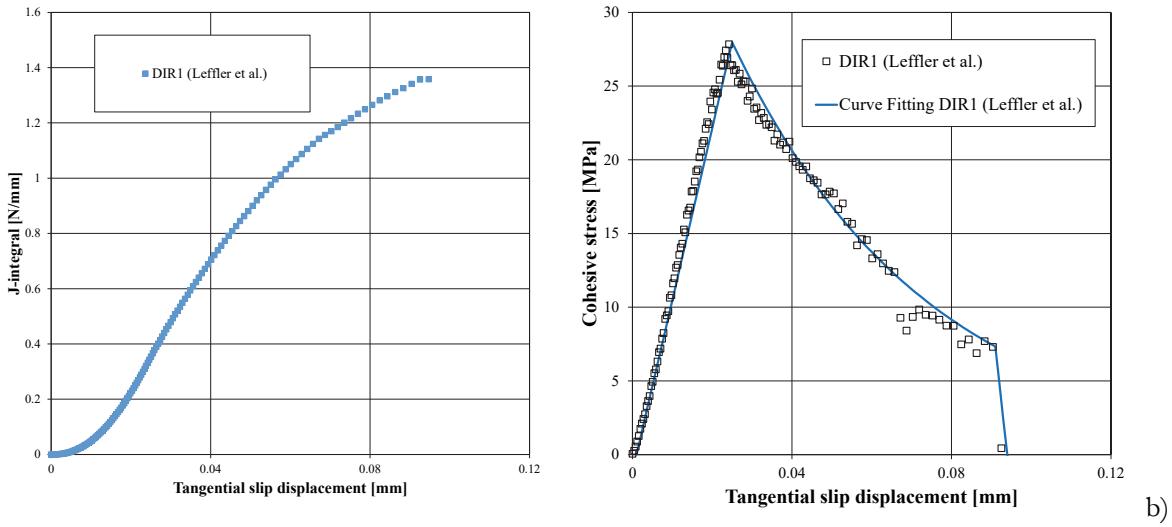

a) b)

Figure 5: a) Trend of J-integral vs tangential slip displacements δ_s; b) Traction-separation law resulting from DIR1 method.

The resulting set of points $J_k(\delta_s)$ was used for calculating the numerical derivative of $J(\delta_s)$, see Fig. 5. The cohesive shear stress is indeed expressed by analytical equation:

$$\tau(\delta_s)=\frac{\partial J(\delta_s)}{\partial \delta_s} \tag{2}$$

Successively, the traction-displacement law can be expressed by means of a single function or a system of equations, which best interpolates the data obtained by Eqn. (2).
Fig. 5.b highlights how adhesive layer behavior can be described by means of three analytical equations, which globally and properly fit the experimental results. These formulas can be easily implemented in a FEM code for predictive purposes. More specifically, the mode II cohesive traction-separation obtained via DIR1 method is expressed by the system:

$$\tau(\delta_s)=\begin{cases} K_0\cdot\delta_s \ , & \delta_s \le \delta_{s\_max} \\ A\cdot e^{-\frac{\delta_s}{d}} \ , & \delta_{s\_max}<\delta_s<\delta_{s\_tr} \\ \tau_{tr}-K_{\mathrm{f}}\cdot\left(\delta_s-\delta_{s\_tr}\right) \ , & \delta_{s\_tr}<\delta_s<\delta_{s\_f} \end{cases} \tag{3}$$

where the term $K_0=\tau_{max}/\delta_{s\_max}$ is the cohesive elastic stiffness and δ_{s_max} is the displacement at the maximum shear stress τ_{max}, whilst the slip displacement δ_{s_f} corresponds to the full damage condition when cohesive stress have null value. The softening behaviour is expressed by coupling an exponential stage, described by the parameters A and d, and a linear branch that better represents the brittle failure of bonded joint. The transition between the two branches of the softening stage occurs at the displacement δ_{s_tr} corresponding to the stress τ_{tr}. The coefficient K_{f} is the final softening rate:

$$K_{\mathrm{f}}=\frac{\tau_{tr}}{\left(\delta_{s\_f}-\delta_{s\_tr}\right)} \tag{4}$$

The values of CZM parameters resulting from identification are reported in Tab. 2. In addition, the critical energy release rate J_c represented by the area under the curve formula (3), calculated using integration between $\delta_s=0$ and $\delta_s=\delta_{s\_f}$, is listed into the same table.

Method	A	d	K_0	δ_{s_max}	τ_{max}	K_f	J_c
DIR1	45.5165	0.0492	1165.20	0.024	27.96	2441.77	1.39

Table 2: Traction-separation law parameters by DIR1 method.

Direct method DIR2: evaluation of exact fracture toughness by cohesive forces

The DIR2 method is instead based on the exact solution for CZM identification of adhesive layers subject to shear load and on the concept of cohesive forces, formulated by Cricrì [21]. Experimental data provided by the load cell and the linear variable displacement transducer (LVDT) of testing machine in addition to results, in terms of displacements and strains, from DIC analysis are necessary. The flowchart of DIR2 approach is depicted in Fig. 6.
From the equilibrium of the cohesive energy density acting on an ENF specimen it follows:

$$\mathcal{Q}(\delta_{sa})=\mathcal{Q}(\delta_{sb})+\frac{9}{16}\cdot\frac{\left(P\cdot a_0\right)^2}{EBh^3}+\frac{3}{8}\cdot\frac{P\cdot\left(\delta_{sa}-\delta_{sb}\right)}{h}-\frac{\left[P\cdot\left(a+\Delta x\right)-16M_b\right]^2}{16EBh^3} \tag{5}$$

where $\mathcal{Q}(\delta_{sa})$ and $\mathcal{Q}(\delta_{sb})$ are respectively the cohesive energy density at the crack tip xa and in a point x_b and Δx is the horizontal distance between the points at x_a and x_b.
The location of the point x_b should be selected sufficiently far from the point x_a, in order to best enhance the accuracy of the approach proposed by Cricrì [21], but far enough away from the mid span, i.e. the loading point, in which there is a significant local deformation occurrence.

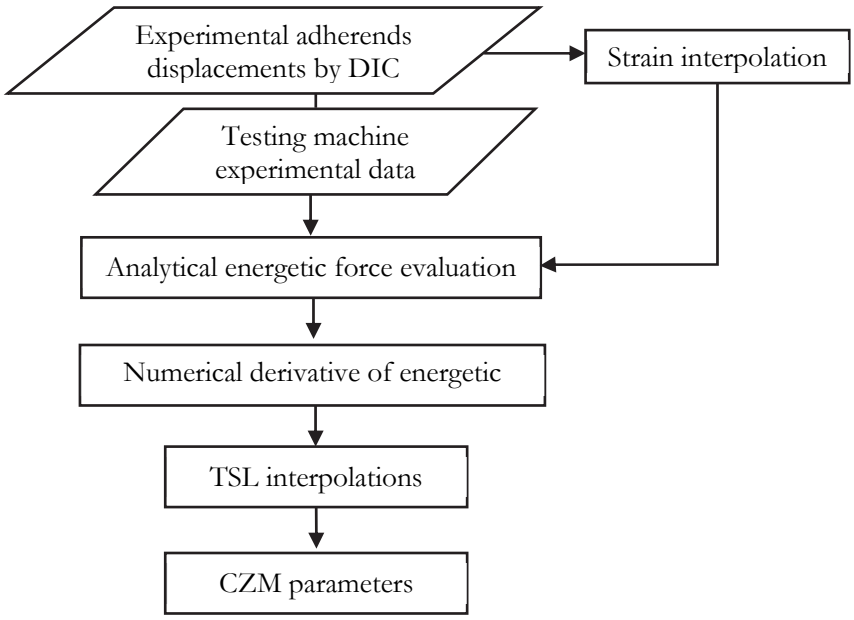

Figure 6: Flowchart of DIR2 approach.

The bending moment at x_b is function of the strain ε_{b2} measured on the bottom of the lower adherend

$$M_b = \frac{EBh^3 \cdot \varepsilon_{b2}}{4h} - \frac{P \cdot (a+L)}{8} \tag{6}$$

The measured strains were fitted with analytical function for reducing the noise related to DIC analysis. Alternatively, the measurement of ε_{b2} can be acquired by traditional strain gauge.

An iterative algorithm was used for the estimation of $Q(\delta_{sa})$. Four iterations were necessary for achieving convergence, as shown in Fig. 7.a. The cohesive traction-separation relationship was then obtained by the derivative of the cohesive energy density at convergence:

$$\tau(\delta_s) = \frac{1}{B} \cdot \frac{\partial Q(\delta_s)}{\partial \delta_s} \tag{7}$$

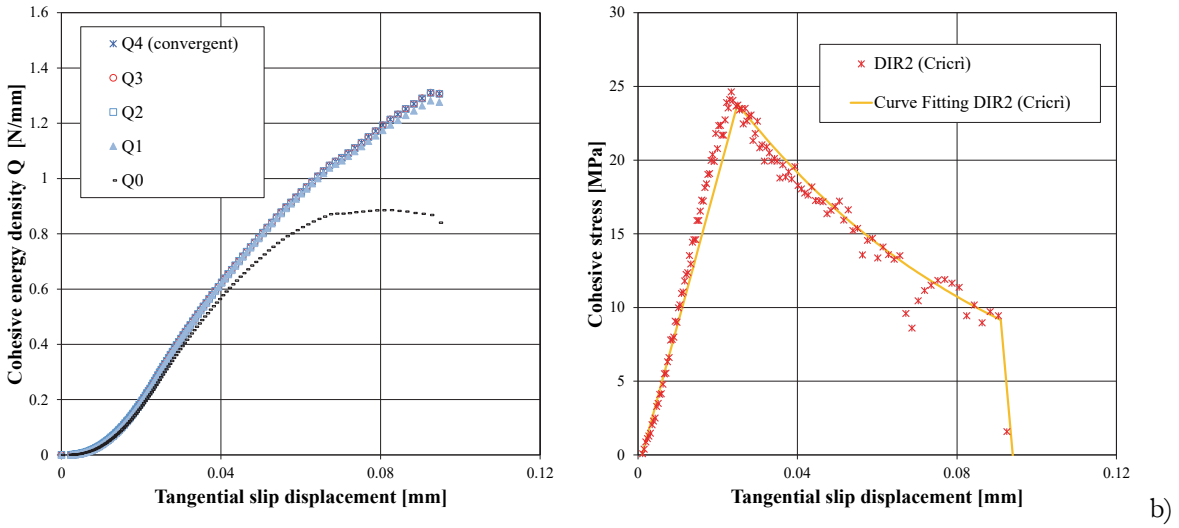

a) b)

Figure 7: a) Trend of cohesive energy density vs tangential slip displacements δ_s; b) Traction separation law resulting from DIR2 method.

Once obtained the points describing interface behavior, a data fitting procedure was assessed for carrying out analytical formulas for elastic and softening stages. The system of Eqns. (3) was also suitable for DIR2 approach outcomes (Fig. 7.b). The identified parameters and the evaluated critical energy release rate are listed in Tab. 3. The maximum value of cohesive shear stress τ_{max} was obtained by finding the point of intersection of the linear and the exponential function of traction-separation law.

Method	A	d	K_0	δ_{s_max}	τ_{max}	K_f	J_c
DIR2	33.6725	0.0691	991.41	0.024	23.79	3052.15	1.34

Table 3: Traction-separation law parameters by DIR2 method.

Direct method DIR3: compliance-based beam approach

The DIR3 method is based on the Compliance-Based Beam Method (CBBM), which relates the strain energy release rate to only compliance variation. The flowchart of DIR3 approach is depicted in Fig. 8.

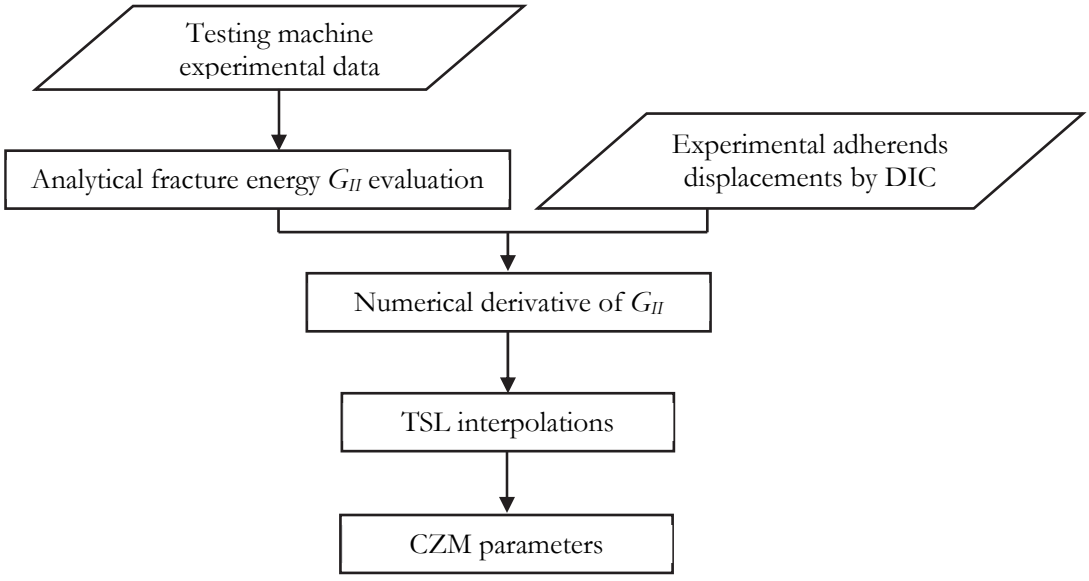

Figure 8: Flowchart of DIR3 approach.

According to de Moura et al. [25] the SERR can be calculated for ENF test with isotropic adherends by equation:

$$G_{II} = \frac{9P^2 \cdot C_{0c}}{2B \cdot \left(3a_0^3 + 2l^3\right)} \cdot \sqrt[3]{\left[\frac{C_c}{C_{0c}} \cdot a_0^3 + \left(\frac{C_c}{C_{0c}} - 1\right) \cdot \frac{2l^3}{3}\right]^2} \tag{8}$$

$$C_c = C - \frac{3l}{10G \cdot B \cdot h} \tag{9}$$

where C_c is the corrected current compliance, C_{0c} is the corrected initial compliance, $C = \delta_p / P$ is the measured compliance, $l = L/2$ is the half span length, P is the applied load, a_0 is the pre-crack length, G is the adherend shear modulus, and B and h are respectively the width and thickness of adherends.Only experimental data from testing machine are necessary to evaluate SERR by means of such a reduction scheme, thus reducing the human errors in measurements of crack length during propagation.

The resulting data set $G_{IIk}(C_c)$ was used for calculating the numerical derivative of points $G_{IIk}(\delta_s)$, reported in Fig. 9.a, taking from experimental data by DIC the values of δ_s corresponding to current crosshead displacement δ_p. The cohesive shear stress is therefore expressed by equation:

$$\tau(\delta_s) = \frac{\partial G_{II}(\delta_s)}{\partial \delta_s} \tag{10}$$

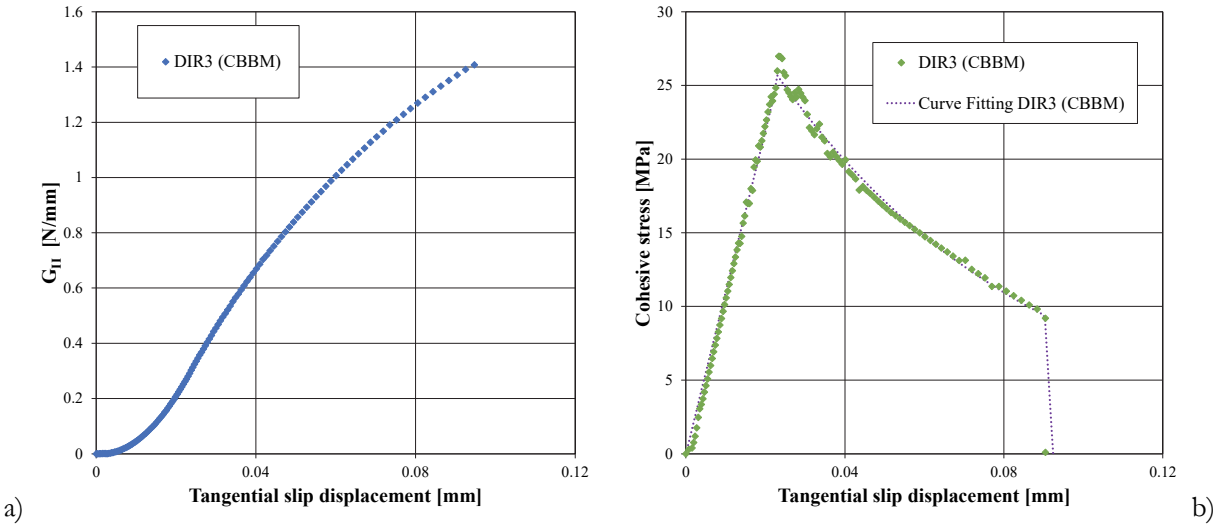

Figure 9: a) Trend of SERR vs tangential slip displacements δ_s; b) Traction separation law resulting from DIR3 method.

The equations system (3) was also suitable for DIR3 method results (Fig. 9.b). The values of CZM parameters resulting from identification are reported in Tab. 4. In addition, the critical energy release rate J_c represented by the area under the curve formula (3), calculated using integration between $\delta_s = 0$ and $\delta_s = \delta_{s\_f}$, is listed into the same table.

Method	A	d	K_0	δ_{s_max}	τ_{max}	K_f	J_c
DIR3	36.2125	0.0669	1095.43	0.0234	26.97	7256.39	1.37

Table 4: Traction-separation law parameters by DIR3 method.

It is worth noting that all the three methods were able to highlight the quasi-brittle behavior of adhesive.

FEM MODEL

A finite element analysis of the ENF test was performed by means of Abaqus software. The overall response resulting from adoption of traction-separation laws as identified by DIR1, DIR2, and DIR3 approaches was carried out and compared. Plane stress assumption was applied, considering the adherends as rigid with respect to the adhesive layer. About 16000 four nodes 2D CPS4 elements were used to model adherend bars. Surface-based cohesive behavior was instead adopted for describing the mode II traction-separation laws via tabular function. Geometric and boundary nonlinearity were included in ENF simulations for modelling the contact between the unbonded surfaces of the specimen, as well as the contact between adherends and supports and that between adherends and loading pin. Being the interface thickness negligibly small, contact cohesive behavior with damage was suitable to model the bonded interface. The contact between adherends in the precrack zone was considered as frictionless. Accurate mesh refinement was performed for achieving convergent solutions. About 2000 elements with aspect ratio equal to the unity modelled the contact region of adherends. Converge analysis was performed using the h-method to reach a tolerance of 0.001 on the percentage difference between tangential slip displacement versus vertical displacements trends.

RESULTS AND DISCUSSION

The lowest critical strain energy release rate J_c resulted in the DIR2 direct methodology. More precisely, the differences between J_c of DIR1 and DIR3 with respect to the one by DIR2 were about 4% and 2%, respectively. On the other hand, the maximum cohesive shear stress τ_{max} by DIR2 resulted smaller of about 18% and 13% than that obtained with the DIR21 and DIR3 methods, respectively. The comparison of identified traction separation laws is presented in Fig. 10. Furthermore, the maximum cohesive shear stress by DIR3 occurred at a tangential slip displacement value approximately 5% smaller than that of DIR2 and DIR1 methods.

The global response of modelled bonded joints is highlighted in Fig. 11 in terms of load-displacement at midspan curve. The maximum force value obtained by using the coefficients of direct methods overestimated the experimental value by about 7%, 5.5%, and 9.5%, respectively with DIR1, DIR2, and DIR3. An initial stiffness greater than the experimental one resulted from all the approaches.

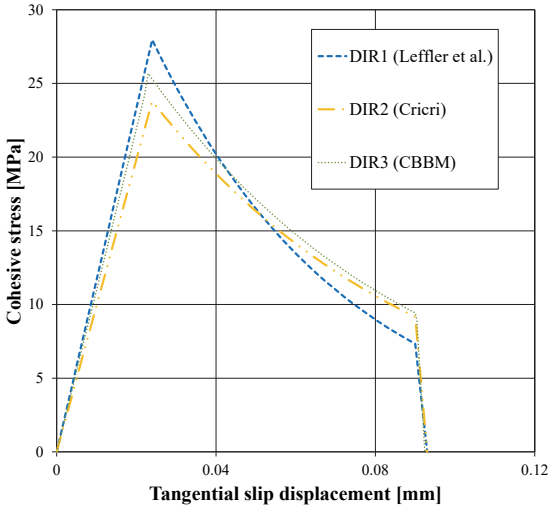

Figure 10: Comparison of identified traction separation laws.

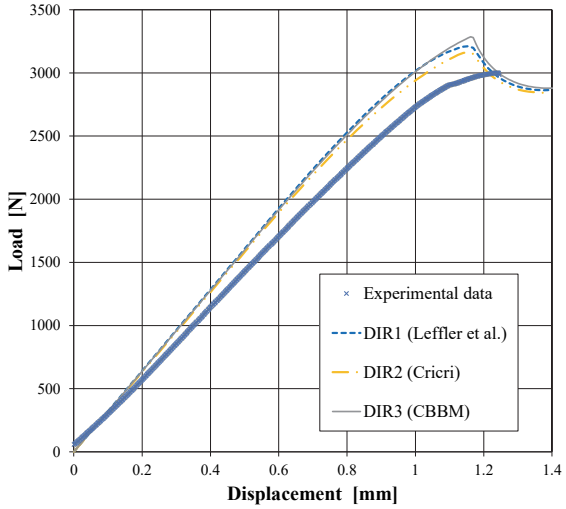

Figure 11: Comparison of load vs displacement curves.

In Fig. 12 the local response is shown in terms of tangential slip displacement of the adhesive layer at the insert tip (position x_a). The CZM predictions by DIR2 approach presents a better agreement in comparison to experimental data rather than those assessed by DIR1 and DIR3 methodologies. Both global and local outcomes highlight that a more accurate evaluation of the critical fracture energy is the basis of a more reliable model of the fracture behavior of bonded joints.

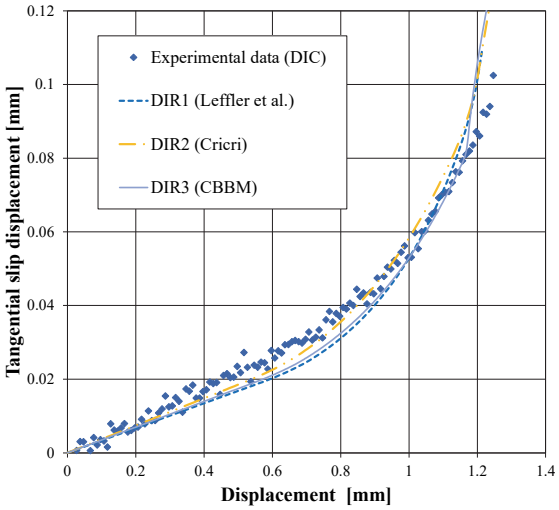

Figure 12: Comparison of interface layer tangential displacements vs vertical displacements at specimen midspan.

The mean square percentage error (MSPE) was used to assess the quality of local response predictions, considering the experimental DIC measurements as reference,

$$MSPE = \frac{1}{n} \cdot \sum_{i=1}^{n} \left(\frac{y_i - \overline{y}_i}{y_i} \right)^2 \tag{11}$$

where y_i is the measure by DIC technique, $\overline{y}_i$ is the FEM result at the same vertical displacement and n is the size of data set. The MSPE resulted in about 16%, 11%, and 14% for DIR1, DIR2, and DIR3 methods, respectively.
Despite a better local and global response, the DIR2 method, requiring an iterative process, needed a greater computational burden for CZM parameters identification than DIR 1 and DIR3 approaches.

CONCLUSIONS

The behavior of adhesive interface layer of bonded joints was investigated in mode II conditions. The use of direct methodology in the identification of CZM law was presented. Three different approaches in fracture energy evaluation were considered and the resulting traction separation relationships were implemented in a FEM code for predictive purposes.
The presented methods require different experimental inputs. In detail, DIR1 needs only load and adhesive interface layer displacement, DIR2 requires load, tangential slip displacement, and flexural strain, whilst load, vertical displacement, and tangential adhesive displacement are necessary for DIR3 approach. The computational effort expected for the identification of the CZM parameters was comparable for DIR 1 and DIR3, while it was higher for DIR2, which uses an iterative process. The global and local response of bonded joint, in terms of load-displacement curve and tangential slip displacements over time respectively, were reported and compared with experimental outcomes. More accurate was the evaluation of strain energy release rate, more sound was the agreement with the experimental response. Indeed, even though there was a 4% maximum difference in critical fracture energy evaluation among the three analyzed direct approaches, the DIR2 was closer to experimental local and global response with respect to DIR1 and DIR3 methodologies. Therefore, the DIR2 method, based on the evaluation of cohesive forces by Cricrì [21], resulted a consistent choice for the prediction of adhesively bonded joints decohesion behavior.

REFERENCES

[1] Campilho, R.D.S.G. (2017). Strength prediction of adhesively-bonded joints, DOI: 10.1201/9781315370835.
[2] D'Ambrisi, A., Mezzi, M., Feo, L., Berardi, V.P. (2014). Analysis of masonry structures strengthened with polymeric net reinforced cementitious matrix materials, Compos Struct, 113(1). DOI: 10.1016/j.compstruct.2014.03.032.
[3] Citarella, R., Cricrì, G. (2014). Three-dimensional BEM and FEM submodelling in a cracked FML full scale aeronautic panel, Applied Composite Materials, 21(3). DOI: 10.1007/s10443-014-9384-5.
[4] Corato, V., Affinito, L., Anemona, A., Vetrella Besi, U. (2015). Detailed design of the large-bore 8 T superconducting magnet for the NAFASSY test facility, Supercond Sci Technol, 28(3). DOI: 10.1088/0953-2048/28/3/034005.
[5] da Silva LFM, Öchsner A, Adams RD, editors. (2011). Handbook of Adhesion Technology. Heidelberg: Springer. DOI: 10.1007/978-3-642-01169-6.
[6] Cricrì, G. (2024). On the determination of the quasi-static evolution of brittle plane cracks via stationarity principle, Comput Methods Appl Mech Eng, 425. DOI: 10.1016/j.cma.2024.116941.
[7] Xu, X.P., Needleman, A. (1993). Void nucleation by inclusion debonding in a crystal matrix, Model Simul Mat Sci Eng, 1(2). DOI: 10.1088/0965-0393/1/2/001.
[8] Gheibi, M.R., Shojaeefard, M.H., Saeidi Googarchin, H. (2019). Direct determination of a new mode-dependent cohesive zone model to simulate metal-to-metal adhesive joints, Journal of Adhesion, 95(10). DOI: 10.1080/00218464.2018.1455145.
[9] Xu, Y., Guo, Y., Liang, L., Liu, Y., Wang, X. (2017). A unified cohesive zone model for simulating adhesive failure of composite structures and its parameter identification, Compos Struct, 182. DOI: 10.1016/j.compstruct.2017.09.012.
[10] Campilho, R.D.S.G., de Moura, M.F.S.F., Pinto, A.M.G., Morais, J.J.L., Domingues, J.J.M.S. (2009). Modelling the tensile fracture behaviour of CFRP scarf repairs, Compos B Eng, 40(2). DOI: 10.1016/j.compositesb.2008.10.008.

[11] Campilho, R.D.S.G., Banea, M.D., Neto, J.A.B.P., Da Silva, L.F.M. (2013). Modelling adhesive joints with cohesive zone models: Effect of the cohesive law shape of the adhesive layer, Int J Adhes Adhes, 44. DOI: 10.1016/j.ijadhadh.2013.02.006.
[12] Fernandes, R.L., Campilho, R.D.S.G. (2019). Accuracy of cohesive laws with different shape for the shear behaviour prediction of bonded joints, Journal of Adhesion, 95(4). DOI: 10.1016/j.compositesb.2016.01.056.
[13] De Sousa, C.C.R.G., Campilho, R., Marques, E.A.S., Costa, M., Da Silva, L.F.M. (2017). Overview of different strength prediction techniques for single-lap bonded joints, in Proceedings of the Institution of Mechanical Engineers, Part L: Journal of Materials: Design and Applications 231. DOI: 10.1177/1464420716675746.
[14] Fernández-Cañadas, L.M., Iváñez, I., Sanchez-Saez, S. (2016). Influence of the cohesive law shape on the composite adhesively-bonded patch repair behaviour, Compos B Eng, 91. DOI: 10.1080/00218464.2018.1438895.
[15] Zhang, J., Wang, J., Yuan, Z., Jia, H. (2018). Effect of the cohesive law shape on the modelling of adhesive joints bonded with brittle and ductile adhesives, Int J Adhes Adhes, 85. DOI: 10.1016/j.ijadhadh.2018.05.017.
[16] Volokh, K.Y. (2004). Comparison between cohesive zone models, Commun Numer Methods Eng, 20(11). DOI: 10.1002/cnm.717.
[17] Silva, D.F.O., Campilho, R.D.S.G., Silva, F.J.G., Carvalho, U.T.F. (2018). Application a direct/cohesive zone method for the evaluation of scarf adhesive joints, Applied Adhesion Science, 6(1). DOI: 10.1186/s40563-018-0115-2.
[18] Li, V.C., Ward, R.J. (1989). A novel testing technique for post peak tensile behaviour of cementitious materials, Fracture Toughness and Fracture Energy, H. Mihashi, H. Takahashi, F.H. Wittmann (Eds.), Fracture toughness and fracture energy: test methods for concrete and rock, CRC Press, Rotterdam.
[19] Sarrado, C., Turon, A., Costa, J., Renart, J. (2016). An experimental analysis of the fracture behavior of composite bonded joints in terms of cohesive laws, Compos Part A Appl Sci Manuf, 90. DOI: 10.1016/j.compositesa.2016.07.004.
[20] Sørensen, B.F., Jacobsen, T.K. (2003). Determination of cohesive laws by the J integral approach, Eng Fract Mech, 70(14). DOI: 10.1016/S0013-7944(03)00127-9.
[21] Cricrì, G. (2019). Cohesive law identification of adhesive layers subject to shear load – An exact inverse solution, Int J Solids Struct, 158. DOI: 10.1016/j.ijsolstr.2018.09.001.
[22] Pereira, F., Dourado, N., Morais, J.J.L., de Moura, M.F.S.F. (2022). A new method for the identification of cohesive laws under pure loading modes, Eng Fract Mech, 271. DOI: 10.1016/j.engfracmech.2022.108594.
[23] Cricrì, G., Perrella, M., Berardi, V.P. (2022). Identification of cohesive zone model parameters based on interface layer displacement field of bonded joints, Fatigue Fract Eng Mater Struct, 45, pp. 821–833. DOI: 10.1111/ffe.13636.
[24] Leffler, K., Alfredsson, K.S., Stigh, U. (2007). Shear behaviour of adhesive layers, Int J Solids Struct, 44, pp. 530–545. DOI: 10.1016/j.ijsolstr.2006.04.036.
[25] de Moura, M.F.S.F., de Morais, A.B. (2008). Equivalent crack based analyses of ENF and ELS tests, Eng Fract Mech, 75, pp. 2584–2596. DOI: 10.1016/j.engfracmech.2007.03.005.